J. Mod. Power Syst. Clean Energy (2014) 2(3):244–255
DOI 10.1007/s40565-014-0071-1

Small signal stability analysis of a synchronized control-based microgrid under multiple operating conditions

Zehan LU, Zhen WANG (✉), Huanhai XIN, Kitpo WONG

Abstract In this paper, a synchronized control strategy of double fed induction generator that can provide reserve capability and primary frequency support for microgrid is firstly developed. The microgrid based small signal stability performance is investigated under multiple operating conditions. The effect of three categories of key controller parameters on dominant eigenvalues is studied by sensitivity analysis, including: 1) active power drooping coefficient; 2) reactive power drooping coefficient; 3) parameters of outer loop excitation current control. Finally, some constructive suggestions on how to tune controller parameters to improve microgrid's small signal stability performance are discussed.

Keywords Microgrid, Synchronized control, DFIG, Small signal stability, Eigenvalues analysis

1 Introduction

In recent years, as an effective means of accommodating renewable energy generation, microgrid technologies are attracting world-wide attention. In a microgrid, wind turbine generators (WTGs) have significant impact on the stable operation of microgrid and energy storage (ES) devices are usually equipped accordingly due to the fluctuation and randomness of wind power output [1].

Although double fed induction generator (DFIG) is one of the most widely installed WTG types, most DFIGs are lacking of regulation capability similar to those conventional synchronous machines (SMs) [2, 3]. This problem is trivial in cases that DFIGs are connected with conventional power grid with a large number of SMs, however it will possibly cause serious frequency stability and power balance problem in microgrid environment characterized as weak equivalent inertia (few rotating elements), small system capacity, high penetration of new energy and large amount of power electronic devices.

There are some publications reported on how to overcome these problems when WTGs are installed in microgrid. One solution is to install ES equipment and improve existing ES control strategies. For example, by introducing synchronized control logic, ES can exhibit some virtual inertia characteristics and compensate for rotating element deficiency in microgrid [4, 5]. However, this solution could result in an increase of overall investment. On the other hand, some works focus on how to improve the existing WTG control strategies. The idea behind is to let DFIG participate in system frequency regulation and thus reduce the ES control effort [6–8]. In [6], droop control is introduced so that DFIG can play primary frequency regulation role. Further in [7], DFIG control uses the system frequency derivative as signal input to emulate some inertial response function. In [9–11], some design schemes for independent power supply to isolated loads are developed for DFIG.

Due to the high volatility of renewable energy generation, the operating conditions in a microgrid environment are very complicated. As a result, the controller parameter design for the purpose of microgrid small signal stability (SSS) enhancement has become a big challenge [12]. In [13], a droop control-based ES in microgrid is designed and the

CrossCheck data: 15 August 2014

Received: 14 June 2014 / Accepted: 4 September 2014 / Published online: 20 September 2014

Z. LU, Z. WANG, H. XIN, College of Electrical Engineering, Zhejiang University, Hangzhou, China
(✉) e-mail: eewangzhen@gmail.com
K. WONG, School of Electrical, Electronic and Computer Engineering, University of Western Australia, Perth, Australia

STATE GRID
STATE GRID ELECTRIC POWER RESEARCH INSTITUTE

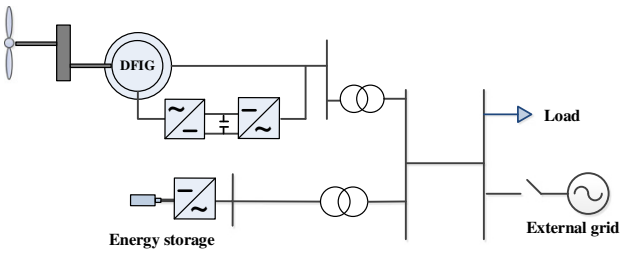

Fig. 1 The topology of the microgrid under study

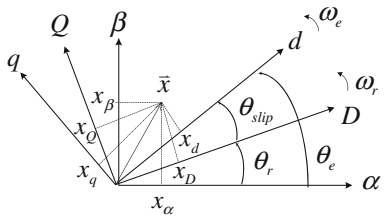

Fig. 2 The *dq* reference frame for DFIG

effect of key ES parameters on SSS performance is discussed. In [14, 15], the effect of DFIG with a constant power control scheme on the SSS performance of a single machine infinite-bus (SMIB) system is preliminarily investigated and an intelligence computational method is applied to optimize the controller parameters. On the whole, most of these studies only consider microgrid as an ES equivalent, i.e., the whole microgrid is treated as some external power source, WTG control strategy details are rarely discussed.

The purpose of this paper is to investigate the effect of WTGs on microgrid SSS performance under multiple operating conditions and hence some suggestions on WTG controller design are discussed. The main work of this paper includes:

1) A synchronized control (SC) strategy that can provide primary frequency support for microgrid is developed with active/reactive power droop controllers introduced. Therefore, the microgrid's capability to withstand load variation can be improved.
2) The small signal model of a typical microgrid composed of DFIG and ES is established. The effect of operating conditions and key controller parameters on the microgrid SSS performance is studied.

2 Microgrid control strategies

The isolated microgrid under study is shown in Fig. 1. The microgrid is composed of one WTG and one ES and they are connected with the microgrid by two step-up transformers. Both of the DFIG and the ES here have similar control strategy and logic, in the following the DFIG control strategy will be elaborated and the ES control scheme will be briefly presented.

2.1 Induction generator modeling

Different from the grid-connected system, the isolated microgrid control scheme adopts a *dq* rotating frame at a speed ω_e (the stator flux speed), as illustrated in Fig. 2. ω_e is not always equal to synchronous speed [9]. For transformation purpose, the other two related reference frame, the stationary reference frame ($\alpha\beta$) and the rotor reference frame (DQ) are also given here [16].

Table 1 Main variables in the control loops

Variables	Representation
v_{dr}/v_{qr}, i_{dr}/i_{qr}	Rotor voltages and currents in *dq* coordinate
v_{ds}/v_{qs}, i_{ds}/i_{qs}, i_{ms}	Stator voltages and currents, equivalent stator excitation current in *dq* coordinate
$v_{s,\mathrm{abc}}$, $i_{s,\mathrm{abc}}$, $v_{r,\mathrm{abc}}$, $i_{r,\mathrm{abc}}$	Three phase stator and rotor voltages, currents
$\psi_{s,\mathrm{abc}}$, ψ_{ds}/ψ_{qs}, ψ_{dr}/ψ_{qr}	abc stator flux, *dq* stator and rotor flux
P, Q	Total active and reactive power
ω_e, ω_r	WTG stator flux speed, machine rotor speed
L_s, L_r, L_m, R_s	Stator, rotor and mutual inductance, stator resistance
θ_e, θ_r, θ_{slip}	Stator flux angle, rotor angle and slip angle

The well-known 4th order induction generator is used in the study. Under the rotating *dq* axis, the voltage and flux-linkage equations of DFIG in per unit system (including the time) can be given as follows

$$\begin{cases} \frac{\mathrm{d}}{\mathrm{d}t}\psi_{ds} = v_{ds} - R_s i_{ds} + \omega_e \psi_{qs} \\ \frac{\mathrm{d}}{\mathrm{d}t}\psi_{qs} = v_{qs} - R_s i_{qs} - \omega_e \psi_{ds} \\ \frac{\mathrm{d}}{\mathrm{d}t}\psi_{dr} = v_{dr} - R_r i_{dr} + (\omega_e - \omega_r)\psi_{qr} \\ \frac{\mathrm{d}}{\mathrm{d}t}\psi_{qr} = v_{qr} - R_r i_{qr} - (\omega_e - \omega_r)\psi_{dr} \end{cases} \tag{1}$$

$$\begin{cases} \psi_{ds} = L_s i_{ds} + L_m i_{dr} = L_m i_{ms} \\ \psi_{qs} = L_s i_{qs} + L_m i_{qr} \\ \psi_{dr} = L_m i_{ds} + L_r i_{dr} \\ \psi_{qr} = L_m i_{qs} + L_r i_{qr} \end{cases} \tag{2}$$

where the meaning of variables is explained in Table 1.

2.2 DFIG rotor side synchronized control

To overcome the early DFIG's lacking of frequency regulation in isolated power system, a novel DFIG supplementary frequency control strategy is developed in [9] to maintain an isolate operation, as illustrated in the rotor

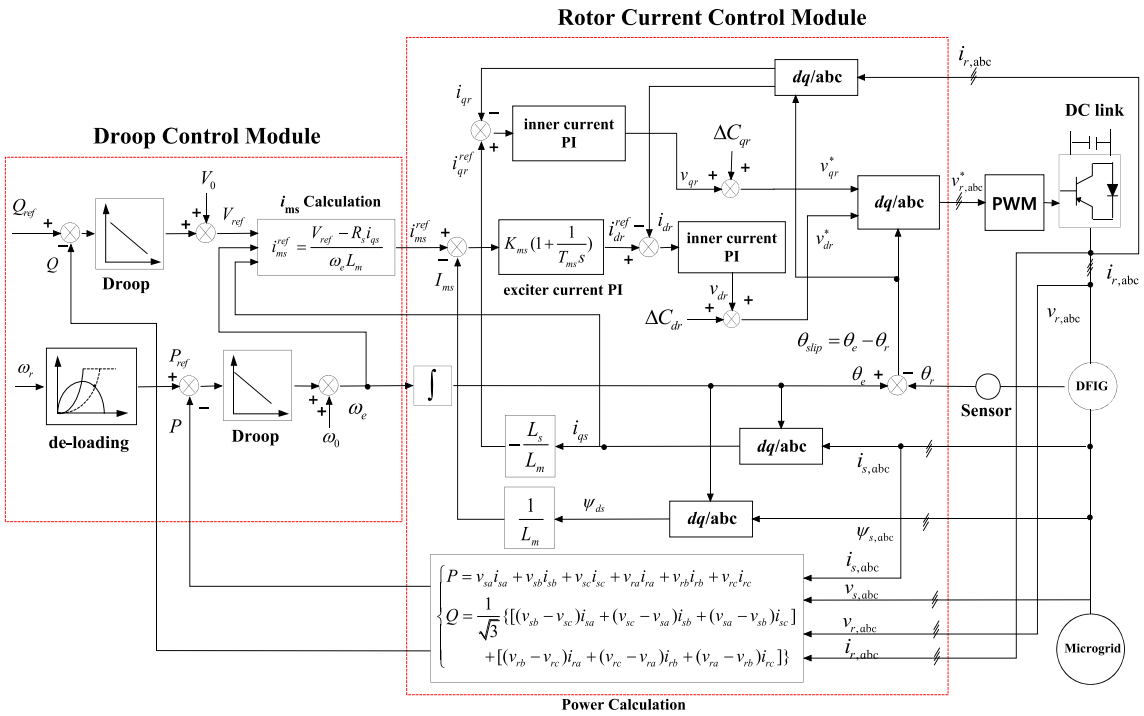

Fig. 3 Synchronized control-based strategy for DFIG rotor side control

current control part of Fig. 3. But this scheme can only set a fixed frequency for each DFIG, which may suffer from potential coordination problem in an isolated microgrid with multiple DFIGs and other power sources.

To solve this problem, in this paper an additional droop control chain is added in the forward path, as shown in the droop control module of Fig. 3. The droop control is used so that DFIG and ES source can share the system load changes and provide frequency support without communication. All variables in Fig. 3 are explained in Table 1.

The concept of SC is to make non-synchronous power sources emulate the synchronous units' function which include power reservation, primary frequency control, secondary frequency control, inertial response, voltage regulation, etc. The whole control scheme shown in Fig. 3 is termed as DFIG synchronized control, as it can provide reserve capability for frequency regulation and synchronization support. By introducing the droop control, the reference value of the stator excitation current i_{ms}^{ref} can be obtained from the external demand, which can realize the decoupling of the stator flux with the microgrid frequency.

For control design purpose, the *d*-axis oriented along the stator flux is used in Fig. 3 and all control variables will ultimately be transformed into the common *dq* reference frame. Considering the difference between the rotating rotor and the stationary stator, a transformation diagram of

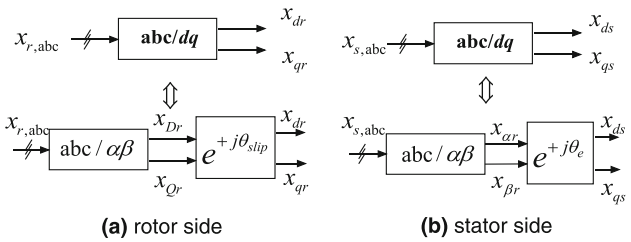

Fig. 4 The reference frame transformation

abc/*dq* on stator and rotor sides is plotted in Fig. 4, their inverse transformation *dq*/abc can be easily derived. All these transformations are also valid to the ES control scheme by using the corresponding ES control variables.

The proposed SC scheme in Fig. 3 is mainly compose of two controllers: a) power droop controller; b) rotor current controller.

2.2.1 *Power droop control*

In the droop control scheme, the WTG stator flux speed command (ω_e) is introduced from the output of the active power droop control, i.e., the active power droop control plays a role of setting the reference value for the stator flux speed. The output of the reactive power droop control gives the command of voltage reference.

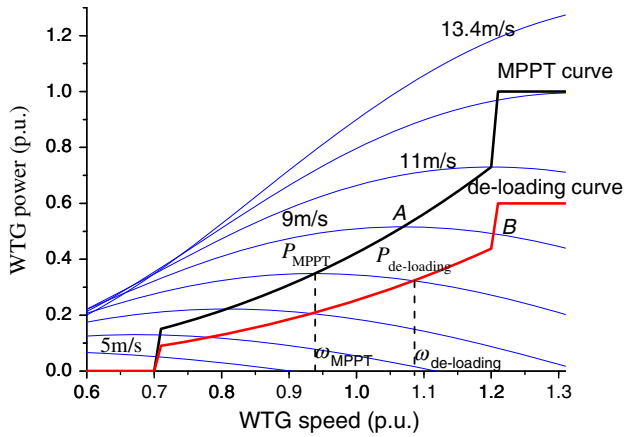

Fig. 5 The frequency de-loading control

The droop control logic can be simply expressed as

$$\begin{cases} \omega_e = \omega_0 + K_P\left(P_{ref} - P\right) \\ V_{ref} = V_0 + K_Q\left(Q_{ref} - Q\right) \end{cases} \tag{3}$$

where ω_0 and V_0 are system rated speed and voltage. Under isolated microgrid operation, the power imbalance can be shared among different droop control power sources. With proper design of droop coefficient K_P and K_Q, new steady control target (ω_e, V_{ref}) can be reached by adjusting P_{ref} and Q_{ref}.

In the active power droop, the de-loading link is of great importance to the synchronized control, with its principle illustrated in Fig. 5. Under the de-loading operation, the DFIG is not operated along the maximum power point tracking (MPPT) curve, but actively along some tracks below the MPPT curve (called de-loading curve) so that part of available wind energy can be store in the form of rotating kinetic energy. As explained in [17], this energy can be released when needed, i.e., the de-loaded power serves as providing additional reserve capability.

A simple linear relationship between MPPT curve and de-loading curve is supposed. Given certain wind velocity, the corresponding power on MPPT point (the intersection between the MPPT curve and the power efficient curve) is denoted as P_{MPPT}, then the corresponding active power reference P_{ref} in the de-loading curve is as follows:

$$P_{ref} = (1 - K_r)P_{MPPT},\ 0 \le K_r < 1 \tag{4}$$

where K_r is the DFIG reserve capability level coefficient. Larger K_r means more frequency regulating capability retained in DFIG, thus better frequency support can be provided.

2.2.2 Rotor current control

On the whole, the rotor side converter (RSC) control scheme consists of two control loops. The inner loop control can regulate the d-axis and q-axis rotor current components, i_{rd} and i_{rq} independently. The outer loop control can regulate the active and reactive power independently [9, 10].

a) The outer loop power control

By adopting the stator flux orientation, it is obvious the following relationships can be obtained from (2):

$$\begin{cases} \psi_{qs} = 0, v_{ds} = 0, v_{qs} = V_m \\ i_{ds} = \frac{L_m}{L_s}(i_{ms} - i_{dr}) \end{cases} \tag{5}$$

where V_m is the grid voltage amplitude.

By substituting (5) into (1), the following expressions can be given,

$$\begin{cases} \frac{L_s}{R_s}\frac{\mathrm{d}}{\mathrm{d}t}i_{ms} + i_{ms} = i_{dr} \\ i_{qs} = \frac{-L_m i_{qr}}{L_s} \end{cases} \tag{6}$$

From (6), an outer loop control law can be derived: 1) the excitation current i_{ms}, which is related to the reactive power, can be controlled by i_{dr} through a proportional-integral (PI) loop, as shown in Fig. 3; 2) the q-axis stator current i_{qs}, which corresponds to the active power, can be controlled by i_{qr}. As a result, the active and reactive power can be controlled independently.

Further, the steady-state form of (1) gives a direct reference signal for the excitation current i_{ms}:

$$i_{ms}^{ref} = \frac{V_{ref} - R_s i_{qs}}{\omega_e L_m} \tag{7}$$

The reference signal for the q-axis stator current i_{sq} is easily given as follows

$$i_{qr}^{ref} = \frac{-L_s i_{qs}}{L_m} \tag{8}$$

b) The inner loop current control

By combining (1) and (2), the RSC control law can be given as follows

$$\begin{cases} v_{dr} = L_r\sigma\frac{\mathrm{d}}{\mathrm{d}t}i_{dr} + R_r i_{dr} + \Delta C_{dr} \\ v_{qr} = L_r\sigma\frac{\mathrm{d}}{\mathrm{d}t}i_{qr} + R_r i_{qr} + \Delta C_{qr} \end{cases} \tag{9}$$

$$\begin{cases} \Delta C_{dr} = \frac{L_m^2}{L_s}\frac{\mathrm{d}}{\mathrm{d}t}i_{ms} - (\omega_e - \omega_r)L_r\sigma i_{qr} \\ \Delta C_{qr} = (\omega_e - \omega_r)\left(\frac{L_m^2 i_{ms}}{L_s} + L_r\sigma i_{dr}\right) \end{cases} \tag{10}$$

where $\sigma = 1 - L_m^2/(L_r L_s)$; ΔC_{dr} and ΔC_{qr} are two forward compensation items and can be ignored in SSS analysis.

Then the rotor voltages v_{dr} and v_{qr} can respectively be controlled by the rotor currents i_{dr} and i_{qr} via two inner loop current PI control links, as can be seen in Fig. 3.

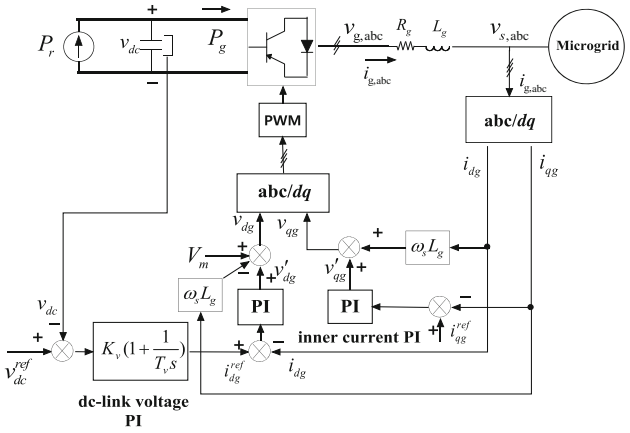

Fig. 6 GSC control scheme

2.3 DFIG grid side converter control

The DFIG grid side converter (GSC) control are usually composed of two cascaded control loops [9, 10]: the inner loop current control regulate independently the d-axis and q-axis grid side current, i_{dg} and i_{qg}; the outer loop control can regulate the dc-link voltage and reactive power exchanged between the GSC and the grid. In the GSC control scheme, the dq axis with the microgrid rotating speed ω_s is adopted for convenience. For sake of independently control of active and reactive power, the d-axis is aligned along the grid (stator) voltage position ($v_{ds} = V_m$, $v_{qs} = 0$) [10]. The GSC control scheme is given in Fig. 6.

2.3.1 The inner loop current control

In Fig. 6, it is obvious that the following ac-side circuit equation holds.

$$v_{g,\mathrm{abc}} = L_g \frac{\mathrm{d}}{\mathrm{d}t} i_{g,\mathrm{abc}} + R_g i_{g,\mathrm{abc}} + v_{s,\mathrm{abc}} \tag{11}$$

The following relationship can be obtained in dq axis:

$$\begin{cases} v_{dg} = R_g i_{dg} + L_g \frac{\mathrm{d}}{\mathrm{d}t} i_{dg} - \omega_s L_g i_{qg} + V_m \\ v_{qg} = R_g i_{qg} + L_g \frac{\mathrm{d}}{\mathrm{d}t} i_{qg} + \omega_s L_g i_{dg} \end{cases} \tag{12}$$

where $\omega_s = 2\pi f_s$ is the microgrid rotating speed.

From (12) it can be derived that v_{dg} and v_{qg} can be regulated by i_{dg} and i_{qg} respectively via two inner current PI links, as shown in Fig. 6.

2.3.2 The outer loop dc-link voltage control

From Fig. 6, it is obvious that when neglecting the losses in the GSC and the circuit, the dc-link circuit has the following power flow equation

$$C_{dc} v_{dc} \frac{\mathrm{d}}{\mathrm{d}t} v_{dc} = P_r - P_g \tag{13}$$

where P_r and P_g are respectively the power from RSC into the DC link and the power flowing into the grid. The purpose of dc-link voltage control is to control the active power exchange in the positive or negative direction between RSC and the microgrid by controlling v_{dc} via feedback loop and the dc-link voltage PI link [9, 10], as illustrated in Fig. 6.

2.3.3 Reactive power control

Theoretically, both RSC and GSC can perform DFIG reactive power regulation function. In the study, the i_{qg}^{ref} is set to zero and the reactive power is dominated by the RSC control.

2.4 ES control

ES in the paper has similar synchronized control logic and structure to that of DFIG RSC control, which is shown in Fig. 7. Here the ES control scheme are also composed of inner loop current control and outer loop active/reactive power control, more details can be found in [17]. Similar to the DIFG RSC case, it should be noted that since the droop control is applied here, so the corresponding frequency command (ω_b) is direct from the output of the active power droop control. In addition, the voltage command is also direct from the output of the reactive power droop control.

3 Microgrid small signal stability analysis (SSSA)

3.1 Induction generator

Followed by (1) and (2), the generator dynamics with stator current and rotor flux as state variables can be given as follows:

$$\begin{bmatrix} \frac{\mathrm{d}}{\mathrm{d}t} i_{ds} \\ \frac{\mathrm{d}}{\mathrm{d}t} i_{qs} \\ \frac{\mathrm{d}}{\mathrm{d}t} \psi_{dr} \\ \frac{\mathrm{d}}{\mathrm{d}t} \psi_{qr} \end{bmatrix} = \begin{bmatrix} D_1 & -\omega_e & -D_2 & -D_3 \\ \omega_e & D_1 & D_3 & -D_2 \\ D_6 & 0 & -D_7 & (\omega_e - \omega_r) \\ 0 & D_6 & -(\omega_e - \omega_r) & D_7 \end{bmatrix} \begin{bmatrix} i_{ds} \\ i_{qs} \\ \psi_{dr} \\ \psi_{qr} \end{bmatrix} + \begin{bmatrix} -D_4 & 0 & D_5 & 0 \\ 0 & -D_4 & 0 & D_5 \\ 0 & 0 & 1 & 0 \\ 0 & 0 & 0 & 1 \end{bmatrix} \begin{bmatrix} v_{ds} \\ v_{qs} \\ v_{dr} \\ v_{qr} \end{bmatrix} \tag{14}$$

where $D_0 = L_m^2 - L_r L_s$; $D_1 = \frac{R_r L_m^2 + R_s L_r^2}{L_r D_0}$; $D_2 = \frac{R_r L_m}{L_r D_0}$; $D_3 = \frac{\omega_r L_m}{D_0}$; $D_4 = \frac{L_r}{D_0}$; $D_5 = \frac{L_m}{D_0}$; $D_6 = \frac{R_r L_m}{L_r}$; $D_7 = \frac{R_r}{L_r}$

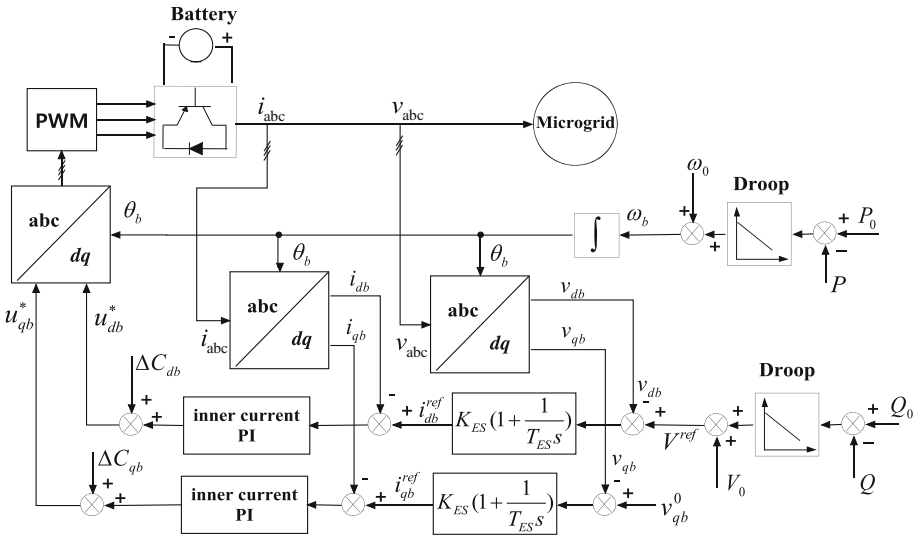

Fig. 7 ES control scheme

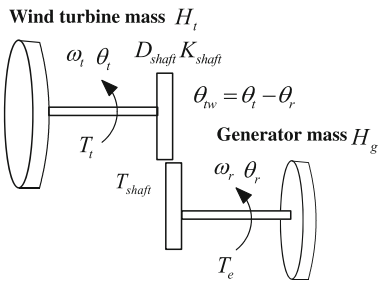

Fig. 8 Two-mass model

3.2 Shaft system model

The two-mass model that can capture the effect of the turbine on the generator is used here, as illustrated in Fig. 8.

$$\begin{cases} \dfrac{\mathrm{d}}{\mathrm{d}t}\theta_{tw} = \omega_t - \omega_r \\ 2H_t \dfrac{\mathrm{d}}{\mathrm{d}t}\omega_t = T_t - T_{shaft} \\ 2H_g \dfrac{\mathrm{d}}{\mathrm{d}t}\omega_r = T_{shaft} - T_e \end{cases} \tag{15}$$

where $T_{shaft} = D_{shaft}(\omega_t - \omega_r) + K_{shaft}\theta_{tw}$; θ_{tw} is the shaft twist angle; H_t and H_g are the turbine and generator inertias, respectively; T_t, T_{shaft} and T_e are respectively the mechanical, shaft and electromagnetic torque.

3.3 Pitch control

The pitch angle control of the blade is activated to prevent overrated power production in strong wind. The pitch control scheme is shown in Fig. 9. The pitch servo dynamics are formulated as follows:

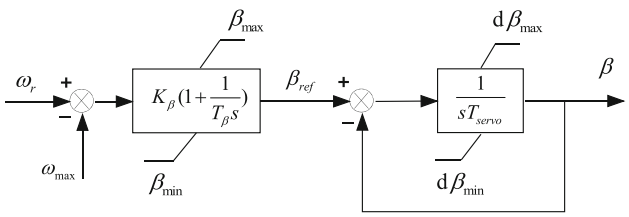

Fig. 9 The pitch control scheme used in the paper

$$\begin{cases} T_\beta \dfrac{\mathrm{d}}{\mathrm{d}t} x_\beta = \omega_r - \omega_{\max} \\ \dfrac{\mathrm{d}}{\mathrm{d}t}\beta = T_{servo}\left[x_\beta + K_\beta(\omega_r - \omega_{\max}) - \beta\right] \end{cases} \tag{16}$$

where K_β and T_β are the pitch control PI coefficients; T_{servo} is the servo system time constant; $\omega_{\max}$ is the maximum rotor speed allowed; β is the pitch angle.

3.4 RSC dynamics

When analyzing the RSC dynamics in Fig. 3, the inner current control dynamic can be omitted due to its well-tracking performance [14]. That means

$$\begin{cases} i_{dr}^{ref} = i_{dr} \\ i_{qr}^{ref} = i_{qr} \end{cases} \tag{17}$$

Accordingly, the RSC dynamic equations are given by

$$\begin{cases} \dfrac{\mathrm{d}}{\mathrm{d}t}\theta_e = \omega_e \\ \dfrac{\mathrm{d}}{\mathrm{d}t}x_{ms} = \dfrac{K_{ms}}{T_{ms}}(i_{ms}^{ref} - i_{ms}) \\ i_{dr}^{ref} = i_{dr} = K_{ms}(i_{ms}^{ref} - i_{ms}) + x_{ms} \end{cases} \tag{18}$$

where K_{ms} and T_{ms} are the PI coefficients of the outer loop exciter current control.

3.5 GSC dynamics

Similarly, the inner loop current control is omitted and the outer loop dc-link voltage control dynamic in Fig. 6 can be expressed as

$$\begin{cases} \dfrac{\mathrm{d}}{\mathrm{d}t}x_v = \dfrac{K_v}{T_v}(v_{dc}^{ref} - v_{dc}) \\ i_{dg}^{ref} = i_{dg} = K_v(v_{dc}^{ref} - v_{dc}) + x_v \end{cases} \tag{19}$$

The dc-link dynamics is obtained directly from (13),

$$C_{dc}v_{dc}\frac{\mathrm{d}}{\mathrm{d}t}v_{dc} = \frac{3}{2}(v_{dr}i_{dr} + v_{qr}i_{qr} - v_{dg}i_{dg} - v_{qg}i_{qg}) \tag{20}$$

3.6 ES dynamics

Similar analysis to DFIG RSC is performed here and the following equations can be obtained from Fig. 7.

$$\begin{cases} \dfrac{\mathrm{d}}{\mathrm{d}t}\theta_b = \omega_b \\ \dfrac{\mathrm{d}}{\mathrm{d}t}x_{db} = \dfrac{K_{ES}}{T_{ES}}(V^{ref} - v_{db}) \\ \dfrac{\mathrm{d}}{\mathrm{d}t}x_{qb} = \dfrac{K_{ES}}{T_{ES}}(v_{qb}^0 - v_{qb}) \\ i_{db}^{ref} = i_{db} = K_{ES}(V^{ref} - v_{db}) + x_{db} \\ i_{qb}^{ref} = i_{qb} = K_{ES}(v_{qb}^0 - v_{qb}) + x_{qb} \end{cases} \tag{21}$$

where K_{ES} and T_{ES} are the PI coefficients of the ES outer loop active/reactive power control.

From (14) to (21), a set of state equations to represent the whole microgrid dynamics in the paper are formulated, which can be further linearized to form the small signal

Table 2 Dominant eigenvalues under different wind speed

Mode	Wind speed (m/s)			Participation factor
	6.5	9	12.5	
$\lambda_{1,2}$	−0.171 ± 10.794j	−0.18 ± 10.797j	−0.07 ± 10.801j	θ_{tw}, ω_t and ω_r, shaft dynamics
λ_3	−2.054	−2.06	−2.132	x_{ms}, DFIG RSC outer loop
λ_4	−11.606	−11.101	−11.319	x_v, DFIG GSC outer loop
$\lambda_{5,6}$	−0.491 ± 0.016j	−0.493 ± 0.017j	−0.496 ± 0.019j	x_{db}, x_{qb}, ES outer loop

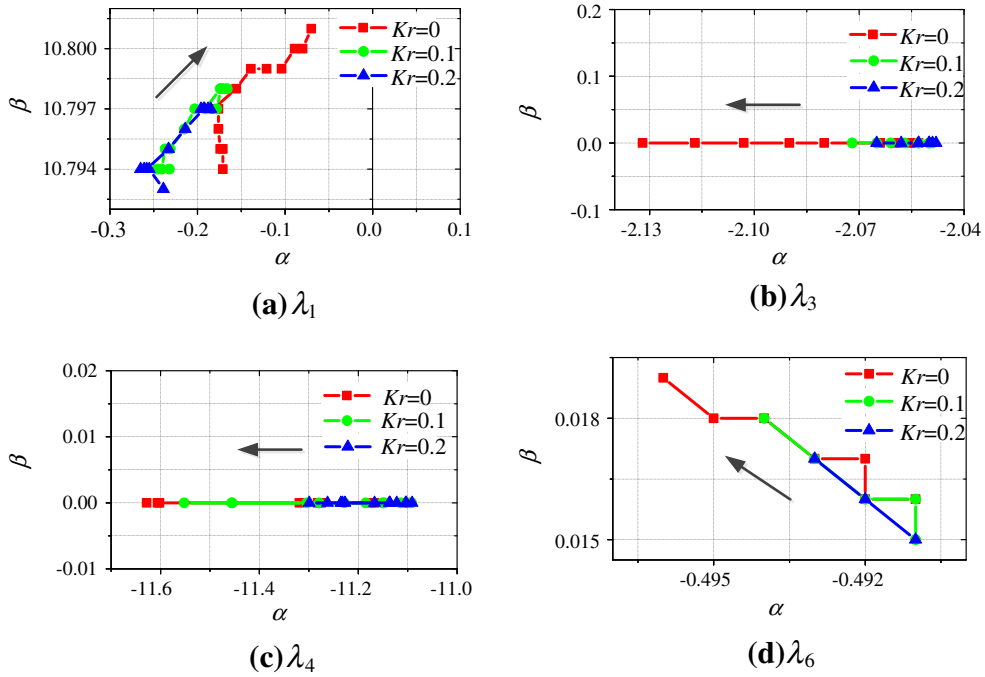

Fig. 10 Dominant eigenvalues locus when wind speed increases from 5 m/s to 14 m/s

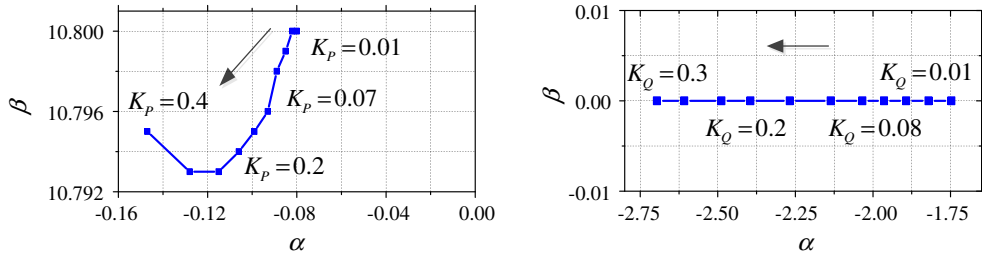

(a) locus of λ_1 as K_P increases **(b)** locus of λ_3 as K_Q increases

Fig. 11 Droop coefficient effect

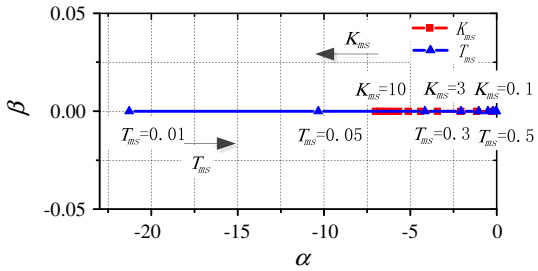

Fig. 12 Locus of eigenvalues λ_3 as K_{ms} and T_{ms} independently increases

models and the eigenvalue analysis can be performed hereinafter.

4 Case studies

Based on the SSSA modelling in Section 3, the microgrid system in Fig. 1 is studied. The rated power of DFIG and ES are 1.55 MW and 1 MW, respectively. The on-site load is 1.0 MW + 0.2 Mvar. Other system data can be referred to in Appendix A.

This section will focus on the effect of operating conditions and RSC controller parameters on the microgrid SSS performance. The effect of GSC controller can be referred to in [14]. Due to similar control logic and structure to DFIG RSC, the ES controller parameters have similar effect to those of DFIG RSC controllers and their details will not be discussed in the paper.

4.1 Effect of operating conditions

Operating condition can determine the initial stead state of dynamic system, thus affect the microgrid SSS performance. In particular, two types of multiple operating conditions are studied here: a) wind speed level; b) reserve capability level.

4.1.1 Wind speed

Three wind speed levels are investigated 1) low speed (6.5 m/s); 2) middle speed (9 m/s); 3) high speed (12.5 m/s). Table 2 only lists the results of those dominant eigenvalues ($\lambda = \alpha + j\beta$) when the DFIG is at MPPT operation ($K_r = 0$).

Further, according to different DFIG reserve levels, $K_r = 0$, 0.1 and 0.2, Fig. 10 gives the dominant eigenvalue locus when wind speed increases from 5 m/s to 14 m/s.

In Table 2, $\lambda_{1,2}$ are shaft related modes and are affected by the wind speed obviously. As can be observed in Table 2 and Fig. 10(a), as the wind speed increases, the damping ratio ($\xi = -\alpha/\sqrt{\alpha^2 + \beta^2}$) or damping has a decreasing tendency. On the other hand, other oscillation modes in Table 2 are related to DFIG and ES controllers and are insignificantly affected by the wind speed.

4.1.2 Reserve capability level

Similarly, it is shown in Fig. 10 that among four oscillation modes K_r has the greatest impact on the shaft modes $\lambda_{1,2}$, while its effect on other modes can be ignored. When more reserve capability is kept (larger K_r), the damping of the shaft modes increases. In other words, WTG's de-loading operation can improve the system SSS performance.

4.2 Effect of RSC controller parameters

Based on the oscillation modes listed in Table 2, three categories of controller parameters are investigated: a) active power droop coefficient; b) reactive power droop coefficient; c) RSC outer loop excitation current control. Sensitivity analysis is performed to analyze the effect of these parameters, by changing one parameter and others being fixed. The wind speed is 11 m/s (high wind speed) and WTG is at MPPT operation.

4.2.1 Droop coefficient K_P

It is found that K_P has much more effect on $\lambda_{1,2}$ than other oscillation modes, while its effect on others can be totally ignored. So here only the locus of λ_1 are given in Fig. 11(a).

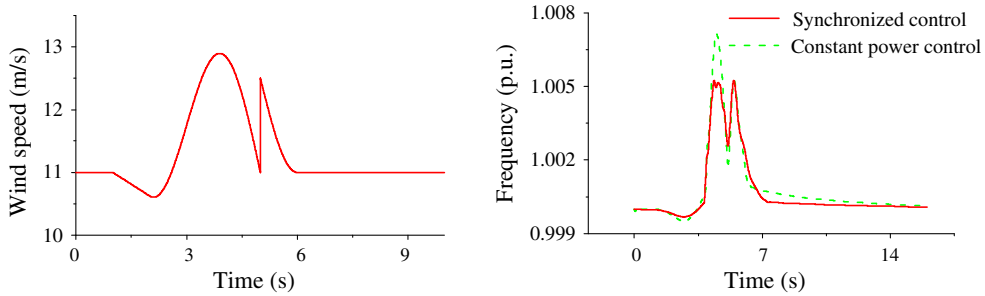

(a) wind speed variation **(b)** frequency response

Fig. 13 The wind speed changes and the corresponding frequency responses

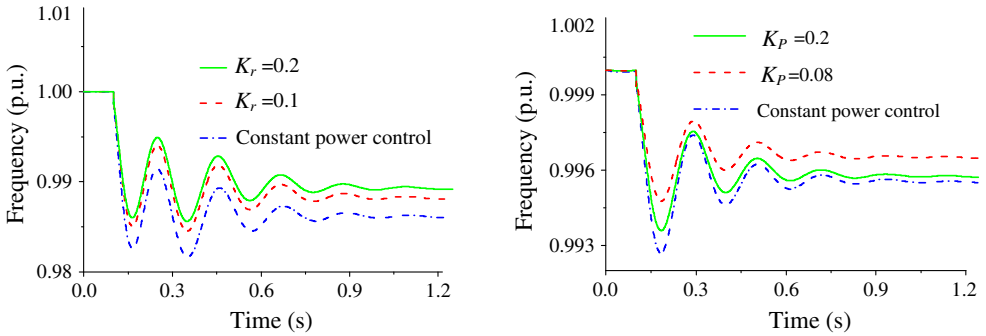

(a) frequency response after load variation with different K_r **(b)** frequency response after load variation with different K_P

Fig. 14 System response after the disturbance

It can be observed that when K_P increases from 0.01 to 0.2, the mode's damping is obviously enhanced, and from 0.2 to 0.4 its damping ratio is slightly reduced. That means K_P need to be carefully tuned for microgrid SSS performance enhancement.

Further study indicate that decreasing the ES's active droop coefficient and keeping DFIG's K_P fixed can have similar effect on λ_1. The reason is that according to the droop control principle the total power output are shared among different power sources according their droop coefficient proportion. That also means careful coordination between droop controllers can more effectively improve the system SSS performance, which can be studied in the future work.

Another potential benefit from the proposed control scheme is that both DFIG and ES can play the role of frequency support and thus the microgrid system can deploy smaller capacity/size ES to maintain the frequency stability compared with those constant power control schemes (e.g. [14, 15]).

4.2.2 Droop coefficient K_Q

The results of sensitivity analysis indicates that only λ_3 is mostly affected by K_Q, which can be well expected since it is an excitation current mode. Its locus are given in Fig. 11(b). It can be seen that increasing of K_Q will greatly enhance the damping of λ_3.

4.2.3 Parameters of RSC excitation current outer loop

The PI coefficients K_{ms} and T_{ms} are investigated. Sensitivity analysis shows that both of them have the most obvious effect on λ_3, and others can be ignored. The locus of λ_3 with respect to these two coefficients are shown in Fig. 12.

It can be observed that increasing K_{ms} will enhance the damping of λ_3, while increasing T_{ms} will reduce the damping. Too small K_{ms} or too large T_{ms} even will make this excitation current mode critical (close to the imaginary axis). Thus careful selection of these two parameters is desired under the microgrid environment.

Some observations and suggestions are summarized based on above discussion:

1) The operating conditions including wind speed and reserve capability level, and the active power droop coefficient have the most obvious effect on shaft modes, but have trivial effect on those controller related modes.

2) On the other hand, the reactive power droop coefficient, and the parameters of RSC outer loop controllers only have obvious effect on the excitation current modes.
3) The above observations indicate that the parameters that have similar effect on the same mode can be grouped and these grouping parameters can be tuned in an coordination way to improve the mode damping, which will obviously facilitate the RSC controller design.

4.3 Simulation validation

The performance of the proposed SC scheme is also compared with a constant power control scheme in [15]. The micro grid data, including those RSC and GSC and ES control scheme data are given in the Appendix A. In the constant power control case, only the RSC adopts the constant power control strategy, while other GSC and ES control schemes and data are the same to the synchronized control case. The control scheme's effectiveness in two cases are studied: a) wind speed variation; b) load disturbance.

4.3.1 Wind speed variation

To consider wind speed variation, the classic three-component wind speed model is used, with the model and data given in the Appendix B. The wind speed changes and the corresponding frequency responses are presented in Fig. 13. It is clear that despite of wind fluctuation, the frequency can still stay stable under both control schemes, but the proposed SC scheme has better frequency recovery performance.

4.3.2 Load disturbance

To simulate a disturbance imposed on the system, a system load increase will be simulated. Here the effect of reserve coefficient K_r and droop coefficient K_P is preliminarily investigated as well.

Suppose there occurs a 50% increase of system load at $t = 0.1$ s, the corresponding frequency responses after disturbance are plotted in Fig. 14a, with $K_r = 0.1$, $K_r = 0.2$ and constant power control respectively considered. On the whole, it can be observed that the proposed SC scheme exhibits better control performance due to its microgrid-isolation oriented design. In addition, it is also shown that higher reserve level (larger K_r) can make the post-disturbance frequency recover better.

Further in Fig. 14b, a 20% increase of system load at $t = 0.1$ s is supposed and scenarios of $K_P = 0.08$ and 0.2 are comparatively studied. In the simulation, K_r is set to 0.1. As shown in the figure, smaller K_P which means more contribution in primary frequency regulation has better frequency recovery performance.

5 Conclusion

An improved synchronized control strategy is developed for the purpose of microgrid SSS enhancement. With the extra frequency support from the DFIG, the microgrid system can deploy smaller capacity/size ES to maintain the frequency stability. Case studies have shown that some categories of controller parameters have independent effect on the microgrid SSS performance and this can help for RSC controller design. Careful coordination between droop controllers can more effectively improve the system SSS performance, and it will be our future work.

Acknowledgement This work is jointly supported by National High Technology R&D Program of China (No. 2011AA050204), the 2014 Endeavour Research Fellowship and 2014 Research Collaborative Award of University of Western Australia, the project of the State Grid (Off-shore wind farm plan in Zhejiang province).

Appendix A

Table A1 DFIG wind turbine parameters

Parameters	Value	Parameters	Value
Rated power/mechanical power, MW	1.55, 1.56	RSC/GSC capacity, MVA	0.6
Wind speed, m/s	11	H_t, H_g, s	3.197, 2.13
Rated stator and rotor voltage, V	690, 1,840	D_{shaft}, K_{shaft}, p.u.	0.346, 0.593
Rated slip	0.0025	R_s, R_r, p.u.	0.0032, 0.0031
DC bus voltage, V	1,150	L_s, L_r, p.u.	1.8169, 1.8037
DC-link capacitor, F	0.015	L_m, p.u.	1.78

Table A2 DFIG control parameters

Parameters	Value	Parameters	Value
Droop coefficients	$K_P = 0.1$, $K_Q = 0.05$	GSC inner loop PI	$K = 1$, $T = 0.01$ s
RSC outer loop PI	$K_{ms} = 1$, $T_{ms} = 0.1$ s	K_β, deg/p.u.	50
RSC inner loop PI	$K = 5$, $T = 1$ s	T_β, T_{servo}, s	0.15, 0.5
GSC outer loop PI	$K_v = 5$, $T_v = 0.1$ s	$\omega_{\max}$, p.u.	1.21

Table A3 ES control parameters

Parameters	Value	Parameters	Value
Rated power, MW	1	Rated AC voltage, V	300
Droop coefficients	$K_P = 0.02$, $K_Q = 0.1$	DC bus voltage, V	800
ES outer loop PI	$K_{ES} = 2$, $T_{ES} = 0.1$ s	ES inner loop PI	$K = 0.2$, $T = 0.01$

Appendix B

The three-component wind speed model is defined by the following equation.

$$V_W = V_{WB} + V_{WG} + V_{WR} \tag{B1}$$

where V_W, V_{WB}, V_{WG} and V_{WR} are the total wind speed, the base speed component (usually constant), the gust speed component and the ramp speed component, respectively.

The gust wind speed component is described by the following equation:

$$V_{WG} = \begin{cases} 0 & t < T_{G0} \\ \frac{V_{G,\max}}{2}\{1 - \cos[2\pi(\frac{t}{T_G} - \frac{T_{G0}}{T_G})]\}, & T_{G0} \le t \le T_{G0} + T_G \\ 0 & t > T_{G0} + T_G \end{cases} \tag{B2}$$

where T_{G0} is the gust start time; T_G is the gust lasting time and $V_{G,\max}$ is the gust peak value.

The ramp wind speed component is modelled by the following equation:

$$V_{WR} = \begin{cases} 0 & t < T_{R0} \\ V_{R,\max}\frac{t - T_{R0}}{T_{R1} - T_{R0}} & T_{R0} \le t \le T_{R1} \\ 0 & t > T_{R1} \end{cases} \tag{B3}$$

where T_{R0}, T_{R1} are respectively the ramp start and end time; $V_{R,\max}$ is the ramp peak value and its positive or negative value corresponds to ramp up or ramp down wind.

The wind parameters used in the paper are given below.

Table B1 Wind speed model parameters

Parameters	Value	Parameters	Value
V_{WB}, m/s	11	$V_{G,\max}$, $V_{R,\max}$, m/s	3, −1.5
T_{G0},T_G, s	2, 4	T_{R0}, T_{R1}, s	1, 5

Reference

[1] Margaris ID, Papathanassiou SA, Hatziargyriou ND et al (2012) Frequency control in autonomous power systems with high wind power penetration. IEEE Trans Sustain Energy 3(2):189–199

[2] Morren J, Haan SWHd, Kling WL et al (2006) Wind turbines emulating inertia and supporting primary frequency control. IEEE Trans Power Syst 21(1):433–434

[3] Hughes FM, Anaya-Lara O, Jenkins N et al (2005) Control of DFIG-based wind generation for power network support. IEEE Trans Power Syst 20(4):1958–1966

[4] Cimuca GO, Saudemont C, Robyns B et al (2006) Control and performance evaluation of a flywheel energy-storage system associated to a variable-speed wind generator. IEEE Trans Ind Electron 53(4):1074–1085

[5] Cardenas R, Pena R, Asher G et al (2004) Power smoothing in wind generation systems using a sensorless vector controlled induction machine driving a flywheel. IEEE Trans Energy Convers 19(1):206–216

[6] Lalor G, Mullane A, O'Malley M (2005) Frequency control and wind turbine technologies. IEEE Trans Power Syst 20(4): 1905–1913

[7] Mauricio JM, Marano A, Gómez-Expósito A et al (2009) Frequency regulation contribution through variable-speed wind energy conversion systems. IEEE Trans Power Syst 24(1): 173–180

[8] Wang Y, Delille G, Bayem H et al (2013) High wind power penetration in isolated power systems-assessment of wind inertial and primary frequency responses. IEEE Trans Power Syst 28(3):2412–2420

[9] Pena R, Clare JC, Asher GM (1996) A doubly fed induction generator using back-to-back PWM converters supplying an isolated load from a variable speed wind turbine. IEE Proc Electr Pow Appl 143(5):380–387

[10] Pena R, Clare JC, Asher GM (1996) Doubly fed induction generator using back-to-back PWM converters and its application to variable speed wind-energy generation. IEE Proc Electr Power Appl 143(3):231–241

[11] Pena R, Cardenasb R, Escobarb E et al (2009) Control strategy for a doubly-fed induction generator feeding an unbalanced grid or stand-alone load. Electr Power Syst Res 79:355–364

[12] Katiraei F, Iravani MR, Lehn PW (2007) Small-signal dynamic model of a micro-grid including conventional and electronically interfaced distributed resources. IET Gener Transm Distrib 1(3):369–378

[13] Rueda JL, Guaman WH, Cepeda JC et al (2013) Hybrid approach for power system operational planning with smart grid and small-signal stability enhancement considerations. IEEE Trans Smart Grid 4(1):530–539

[14] Yang LH, Xu Z, Ostergaard J et al (2011) Oscillatory stability and eigenvalue sensitivity analysis of a DFIG wind turbine system. IEEE Trans Energy Convers 26(1): 328–339

STATE GRID
STATE GRID ELECTRIC POWER RESEARCH INSTITUTE

[15] Yang LH, Yang GY, Xu Z et al (2010) Optimal controller design of a doubly-fed induction generator wind turbine system for small signal stability enhancement. IET Gener Transm Distrib 4(5):579–597
[16] Abad G, López J, Rodríguez M et al (2011) Doubly fed induction machine modeling and control for wind energy generation. Wiley, London
[17] Rocabert J, Luna A, Blaabjerg F et al (2012) Control of Power Converters in AC Microgrids. IEEE Trans Power Electron 27(11):4734–4749

Zehan LU was born in Hebei, China in 1986. He obtained his Bachelor's degree in the College of Electrical Engineering, Southeast University, China, in June 2009. He is currently working towards the Ph.D. degree in the College of Electrical Engineering, Zhejiang University, China. His research interests include renewable energy and power system stability analysis.

Zhen WANG received his B.Sc, M.Sc and Ph.D degree from the Xi'an Jiaotong University, Zhejiang University and Hong Kong Polytechnic University in 1998, 2001 and 2009, respectively. Then he joined Zhejiang University and currently is an associate professor. He was the 2014 Australia Endeavour Research Fellowship recipient and the visiting scholar in the University of Western Australia during February-August 2014. His research interests include power system stability and control, computational intelligence and renewable energy.

Huanhai XIN was born in Jiangxi, China in 1981. He has been with the faculty, currently an associate professor in the department of Electrical Engineering, Zhejiang University, China, after he obtained the Ph.D. degree from the same department in June 2007. He was a post-doctor in the EECS department of the University of Central Florida from June 2009 to July 2010. His research interests include power system stability analysis, and renewable energy.

Kitpo WONG (M'87–SM'90–F'02) received the M.Sc, Ph.D., and higher doctorate D.Eng. degrees from the University of Manchester, Institute of Science and Technology, Manchester, U.K., in 1972, 1974, and 2001, respectively. Since 1974, he has been with the School of Electrical, Electronic and Computer Engineering, The University of Western Australia, Perth, Australia, where he is currently a Winthrop Professor. His current research interests include power system analysis, planning and operations, and smart grids. Prof. Wong received three Sir John Madsen Medals (1981, 1982, and 1988) from the Institution of Engineers Australia, the 1999 Outstanding Engineer Award from IEEE Power Chapter Western Australia, and the 2000 IEEE Third Millennium Award. He was General Chairman of IEEE/CSEE PowerCon2000 conference. He was an Editor-in-Chief of IEE Proceedings in Generation, Transmission and Distribution. Currently he is serving as Editor-in-Chief for IEEE POWER ENGINEERING LETTERS.